Supporting information

Interfacial Electronic Engineering in an Amorphous NiFe LDH/Low-Crystalline CoP_x Heterostructure for Efficient Water Splitting

Minghui Quan,[a] *Yunxiang Liu*[a], *Zufeng He*[a], *Qian Hu*[a],*Abebe Reda Woldu,**[,a] *and Liangsheng Hu**[,a b]

Addresses
[a] Department of Chemistry and Key Laboratory for Preparation and Application of Ordered Structural Materials of Guangdong Province, Shantou University, Guangdong, 515063, PR China
[b] Chemistry and Chemical Engineering Guangdong Laboratory, Shantou, 515063, PR China

Corresponding authors: Abebe Reda Woldu(woldu@stu.edu.cn); Liangsheng Hu (lshu@stu.edu.cn)

Experimental Section

Synthesis of CoP_x Catalyst

A plating solution containing cobalt ions was prepared by dissolving 5.26 g of sodium chloride, 0.95 g of citric acid, 0.63 g of cobalt sulfate, 1.45 g of ammonium fluoride, and 0.50 g of sodium hypophosphite in 50 mL of distilled water, followed by stirring with a glass rod until completely dissolved. Electrochemical deposition of CoPx was then carried out in a three-electrode configuration, using a 0.5 × 2 cm^2 carbon cloth (CC) as the working electrode, a saturated calomel electrode (SCE) as the reference electrode, and a carbon rod as the counter electrode. The deposition was performed using a chronopotentiometric (CP) method at a current density of 3.6 A cm^{-2} for 240 s.

Synthesis of NiFe LDH Catalyst

First, an electrolytic solution was prepared in 100 mL of distilled water containing nickel and iron ions in a concentration ratio of 1:5 (total metal ion concentration of 30 mM). Then, a three-electrode system was employed using Ag/AgCl as the reference electrode, a Pt foil as the counter electrode, and CC as the working electrode. Finally, the NiFe LDH was synthesized on CC through electrodeposition at -1 V for 300 seconds.

Synthesis of NiFe LDH/CoP_x Catalyst

The NiFe LDH/CoP_x heterostructure was synthesized through a two-step electrochemical deposition process. First, CoP_x was electrodeposited onto carbon cloth (CC) following the procedure described earlier. Subsequently, NiFe LDH was deposited onto the as-prepared CoP_x using the same method employed for pristine NiFe LDH. The resulting NiFe LDH/CoP_x heterostructure was then washed with distilled water and ethanol and dried in an oven at 60°C overnight.

Electrochemical performance testing

The electrocatalytic performance for overall water splitting of the catalyst was evaluated in a three-electrode system using a CHI660E potentiostat. The catalyst served

as the working electrode, with a platinum (Pt) wire or carbon rod as the counter electrode, and a saturated calomel electrode (SCE) as the reference electrode. All electrochemical tests employed self-supporting electrodes with a geometric area of 0.25 cm^2 (0.5 × 0.5 cm^2). This size was chosen for material uniformity and was used consistently across all experimental and control samples to ensure valid comparisons. Current densities are reported normalized to geometric area. All measurements were conducted in a 1 M KOH (pH = 13.9) alkaline electrolyte at room temperature. Before the electrochemical measurements, the electrolyte was purged with nitrogen gas for 15 minutes to remove dissolved gases. The catalyst's performance was assessed using linear sweep voltammetry (LSV) with a scan rate of 5 mV s^{-1}. Double-layer capacitance was determined via cyclic voltammetry (CV) at scan rates of 10, 20, 30, 40, and 50 mV s^{-1} within a non-Faradaic potential range. Electrochemical impedance spectroscopy (EIS) was employed to measure the electron transfer resistance of the catalyst, using a frequency range of 0.1–100 kHz. For comparison group catalysts, the potential corresponding to a current density of 10 mA cm^{-2} from the polarization curve of the best-performing catalyst was used as the test voltage. Stability was evaluated using the chronopotentiometry (CP) method at a current density of 1,000 mA cm^{-2}.

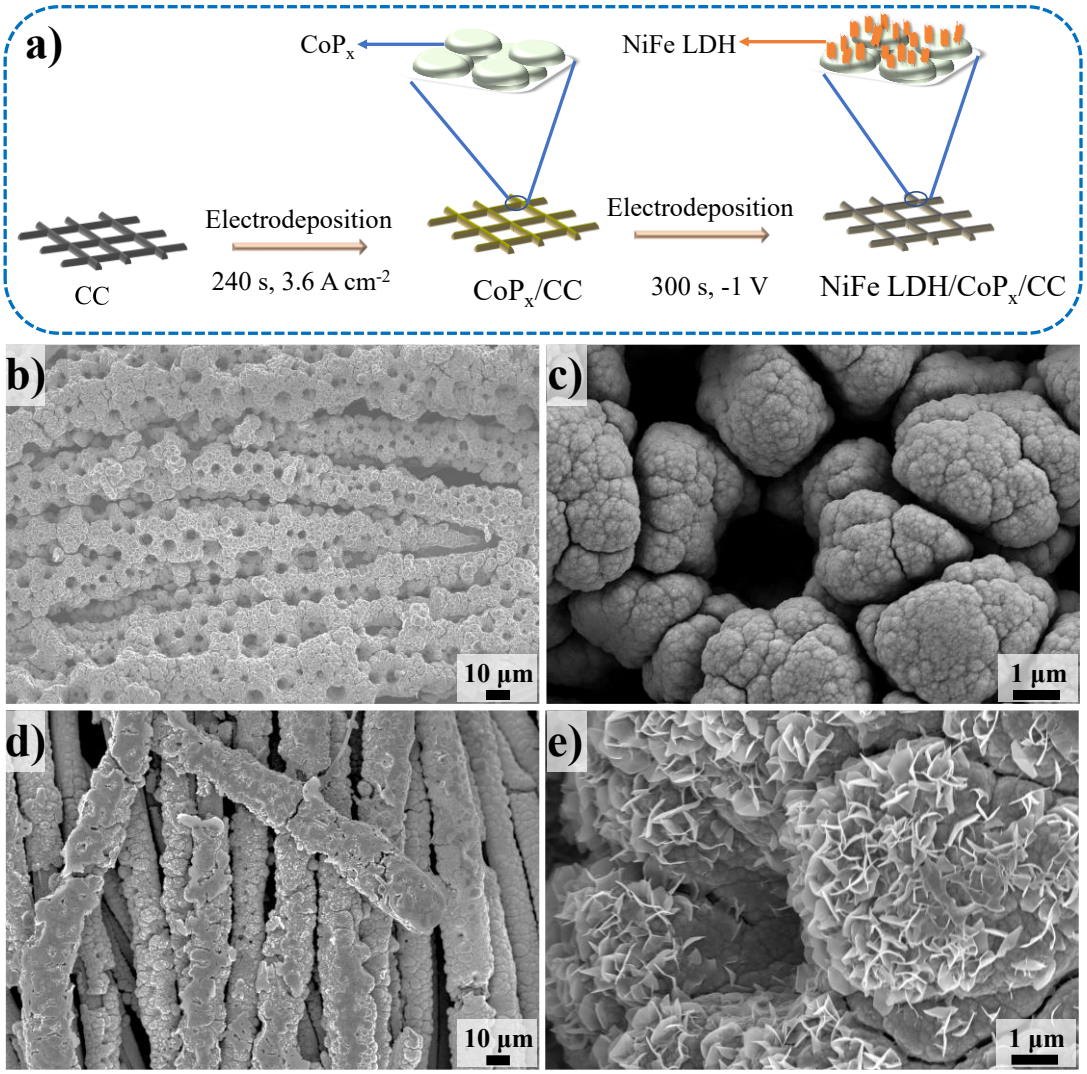

Fig. S1. a) Schematic representation of the electrode preparation, SEM images of b-c) CoP_x, and d-e) NiFe LDH/CoP_x.

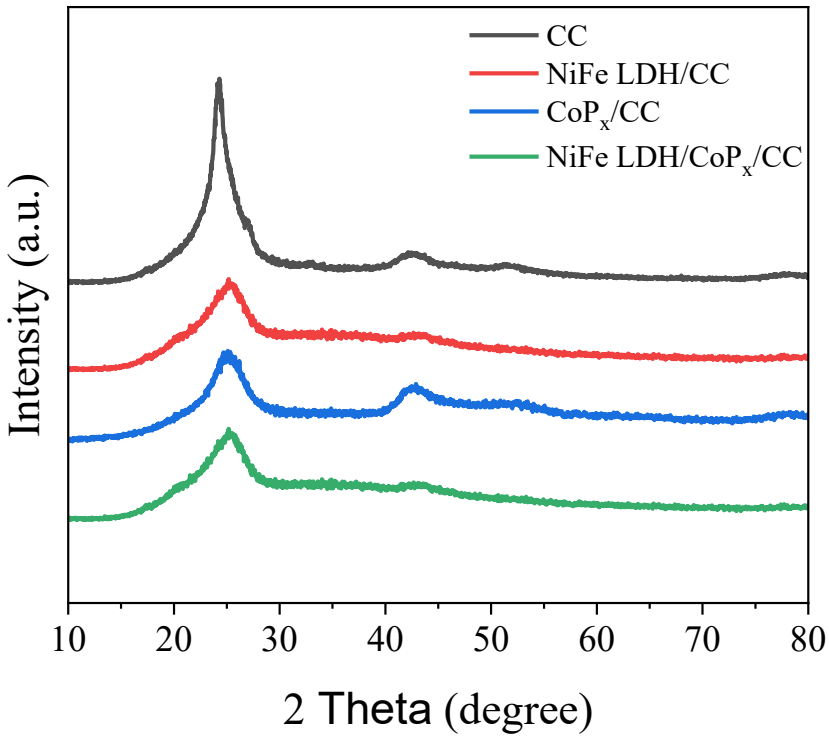

Fig. S2. The XRD patterns of CC, NiFe LDH/CC, CoP_x/CC, NiFe LDH/CoP_x/CC.

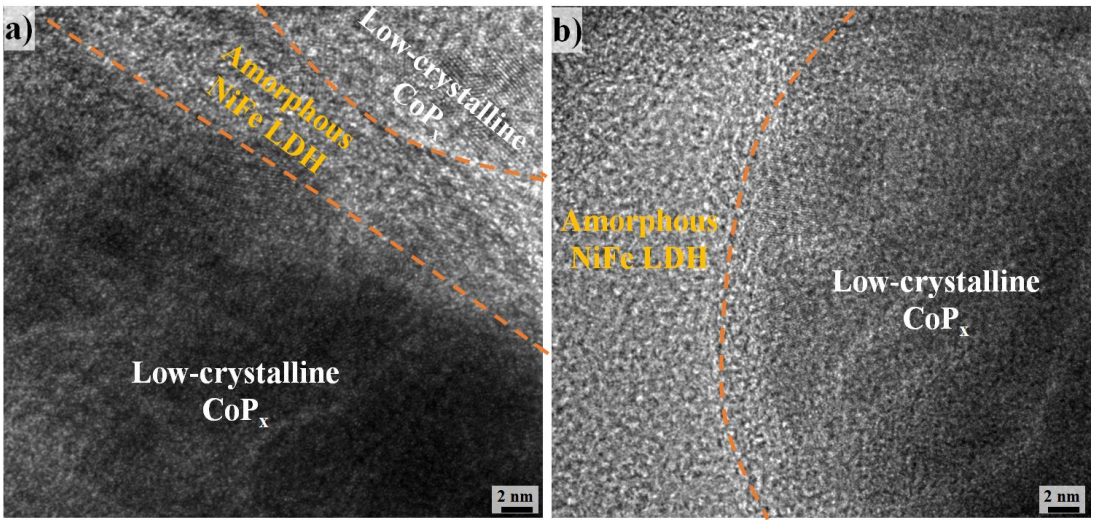

Fig. S3. HRTEM of NiFe LDH/CoPx.

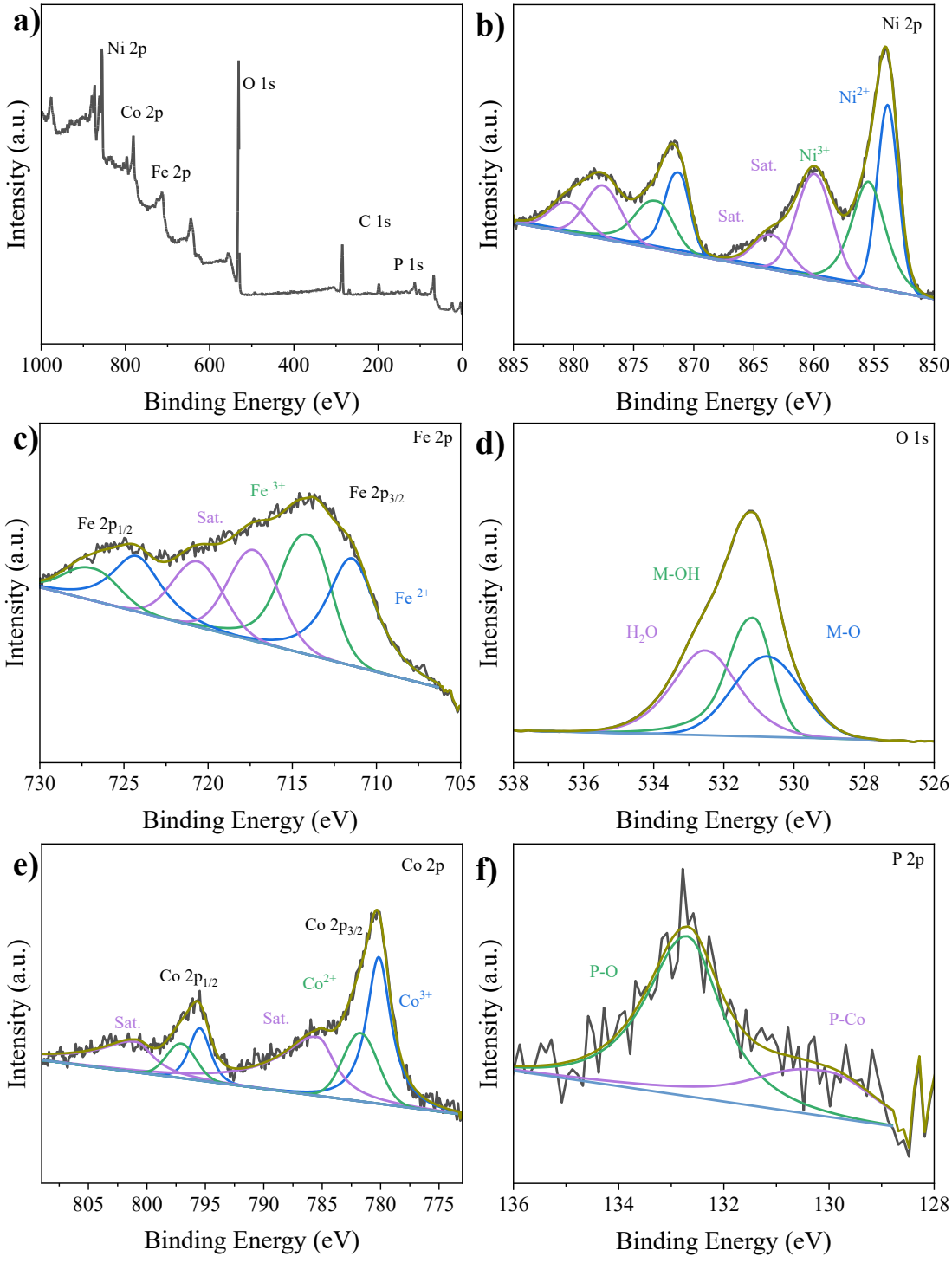

Fig. S4. XPS spectra of NiFe LDH/CoPx a) survey spectrum, b) Ni 2p, c) Fe 2p, d) O 1s, e) Co 2p, and f) P 2p.

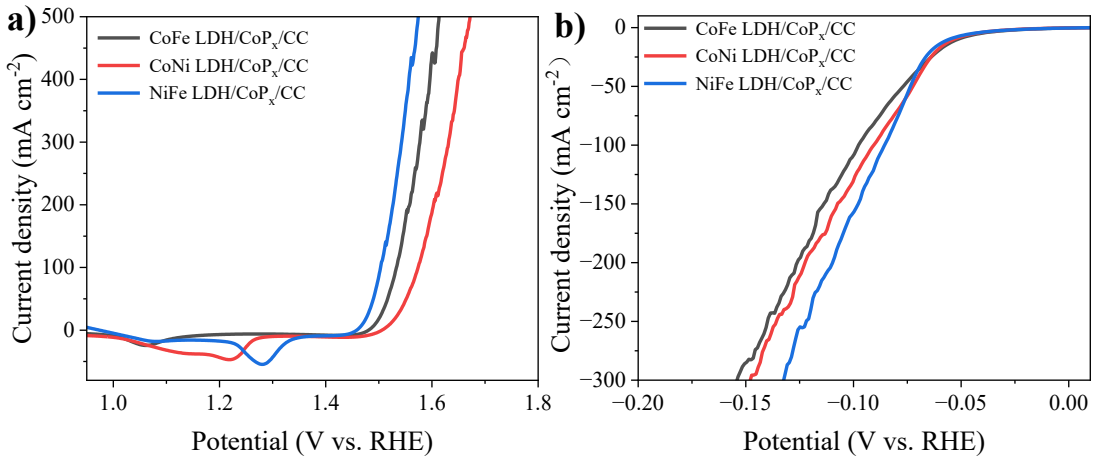

Fig. S5. Screening of different layered double hydroxide (LDH) electrocatalysts heterostructured with CoP_x (CoFe LDH/CoP_x, CoNi LDH/CoP_x, and NiFe LDH/CoP_x) based on a) OER and b) HER polarization curves.

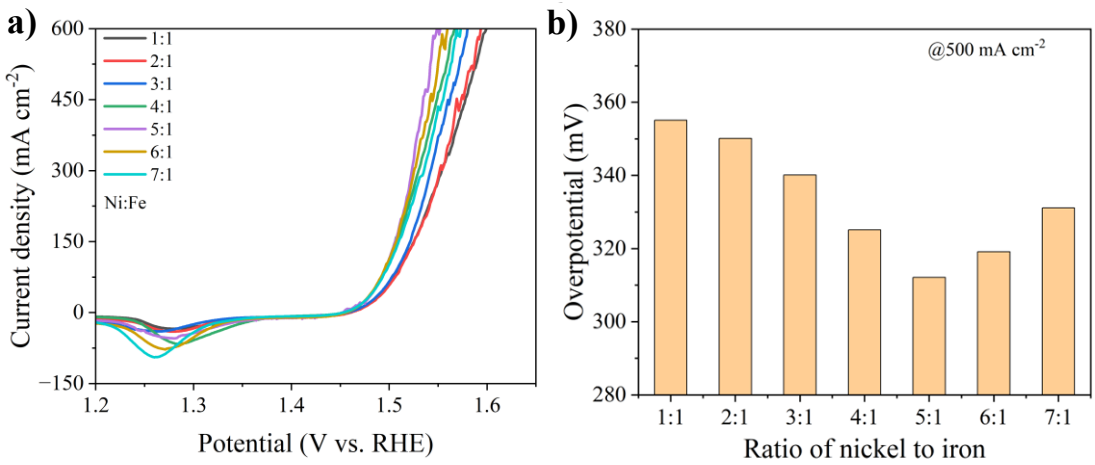

Fig. S6. Optimization of the Ni and Fe ratios of the NiFe LDH in the heterostructured electrocatalysts (NiFe LDH/CoP_x) through LSV measurements in 1 M KOH a) OER polarization curve and b) Overpotential at 500 mA cm^{-2}.

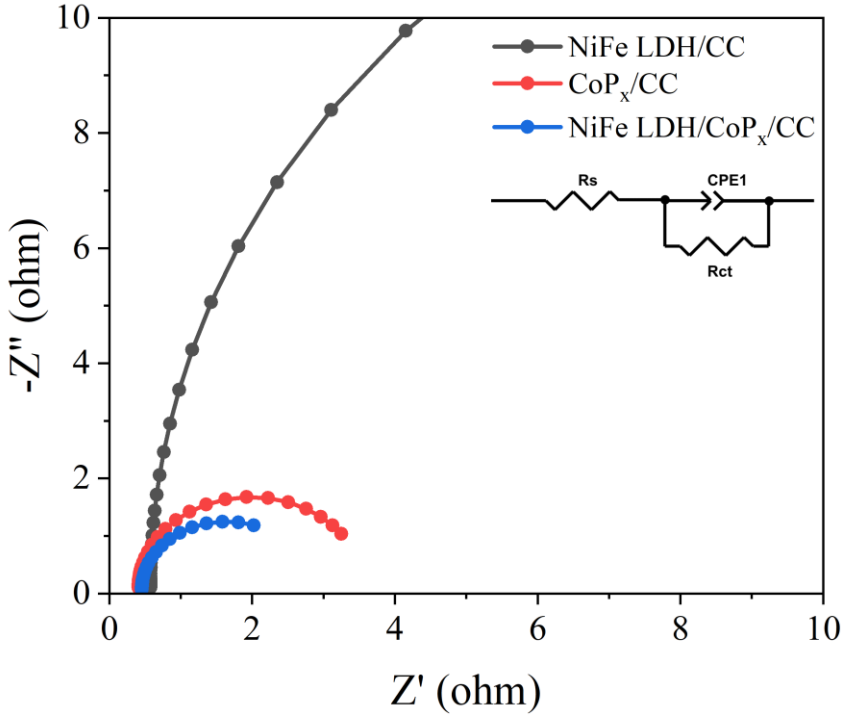

Fig. S7. Nyquist plots of NiFe LDH/CoP_x, NiFe LDH, and CoP_x, respectively, conducted at a voltage of 1.49 V vs. RHE.

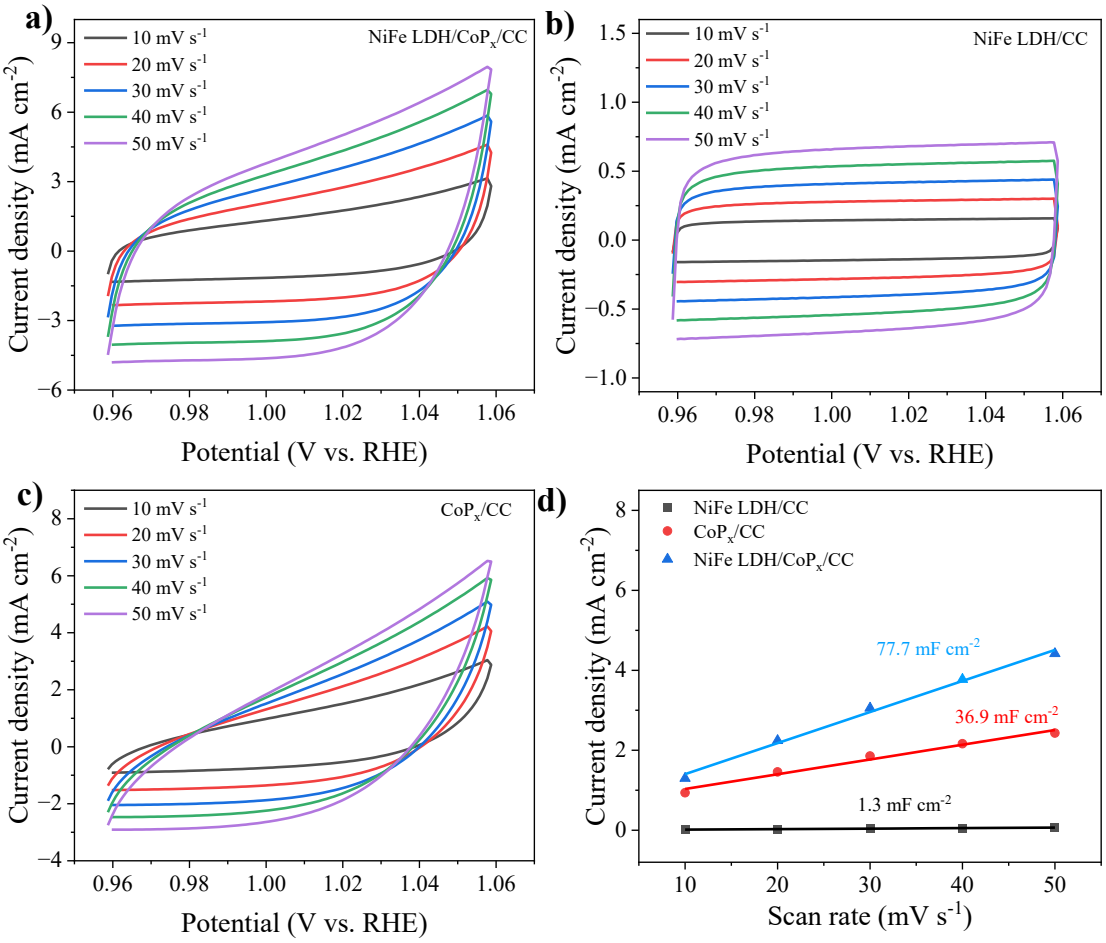

Fig. S8. CV curves at different scanning speeds of a) NiFe LDH/ CoP_x, b) NiFe LDH, c) CoP_x, respectively, and d) C_{dl}.

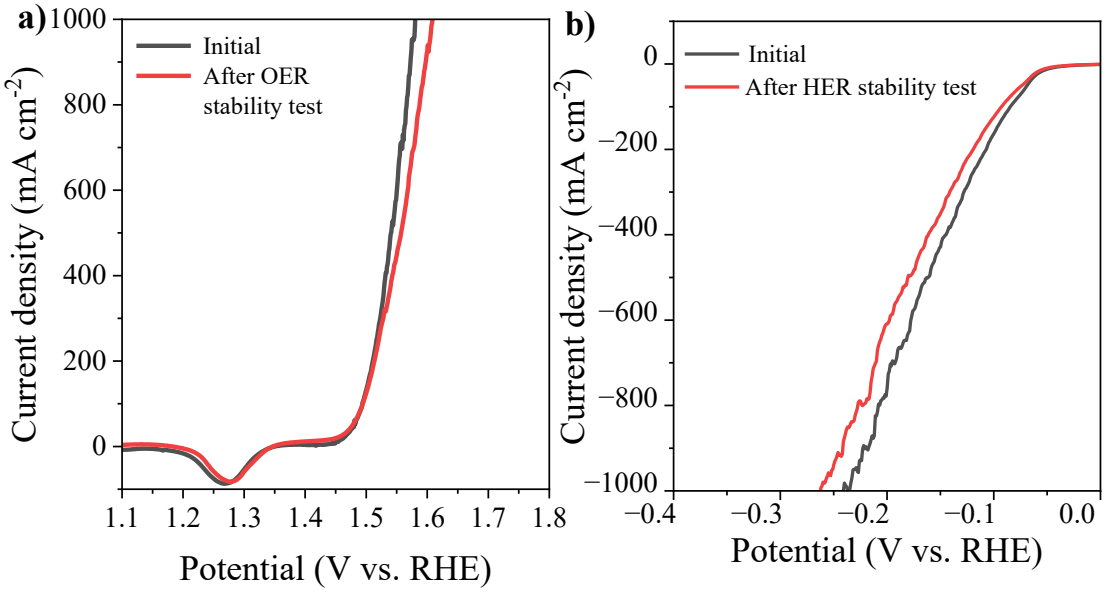

Fig. S9. LSV polarization curve of NiFe LDH/CoP_x before and after the stability test at a current density of 1000 mA cm^{-2} a) OER and b) HER.

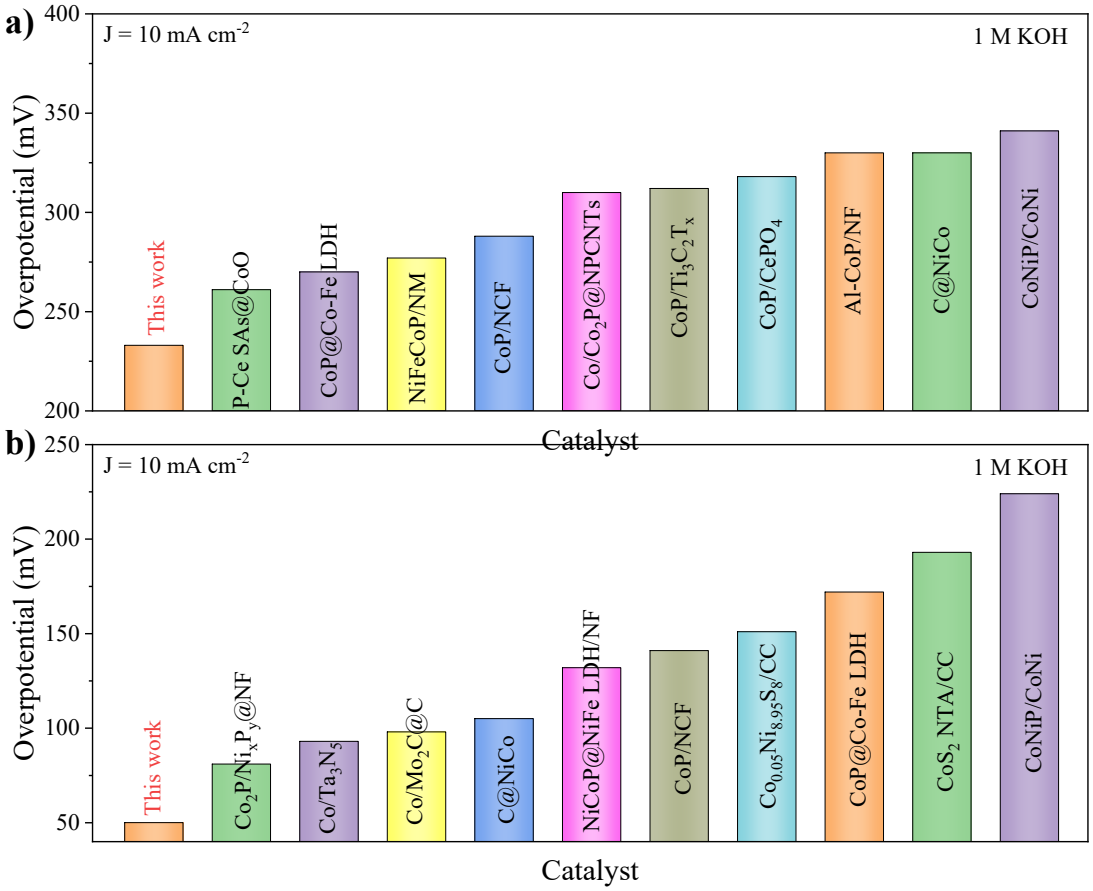

Fig. S10. a) Comparison of OER performance with other cobalt-based catalysts,[1-10] and b) Comparison of HER performance with other cobalt-based catalysts,[1, 2, 4, 8, 11-16].

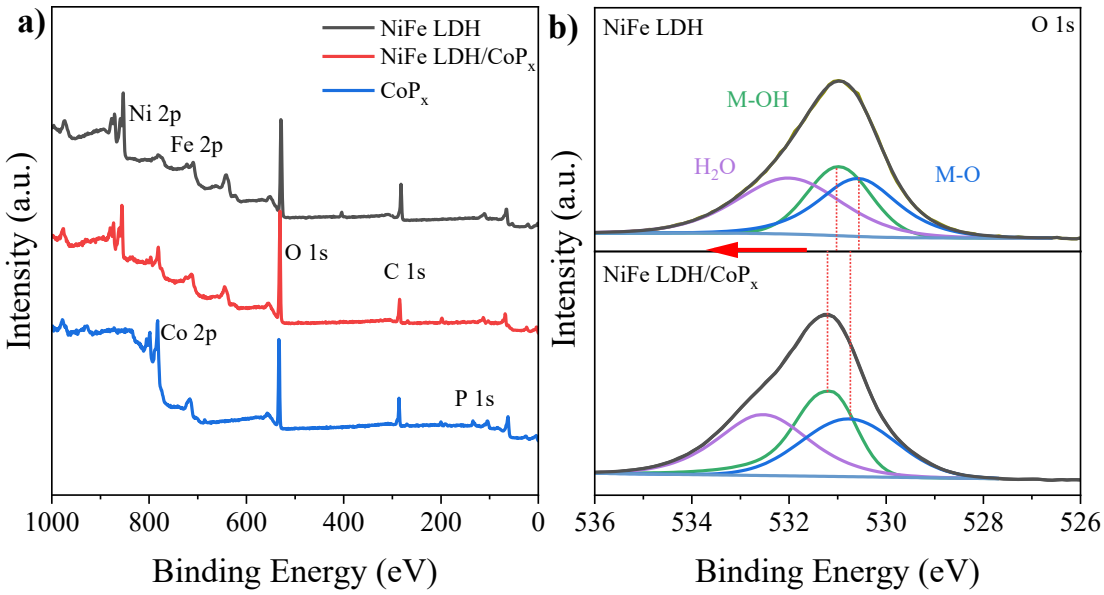

Fig. S11. a) XPS survey spectra of NiFe LDH, CoP_x, and NiFe LDH/CoP_x, and b) the spectra of O 1s.

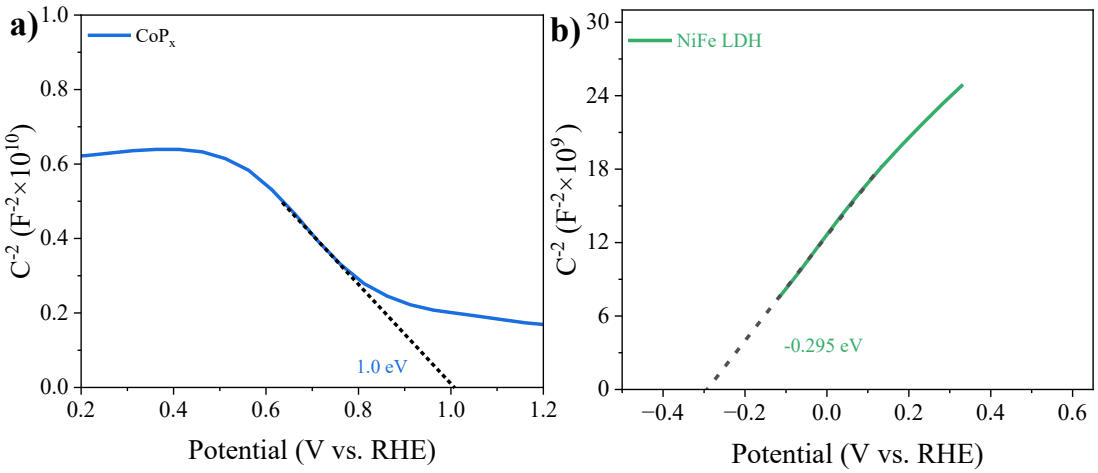

Fig. S12. Mott-Schottky curves of a) CoP_x and b) NiFe LDH.

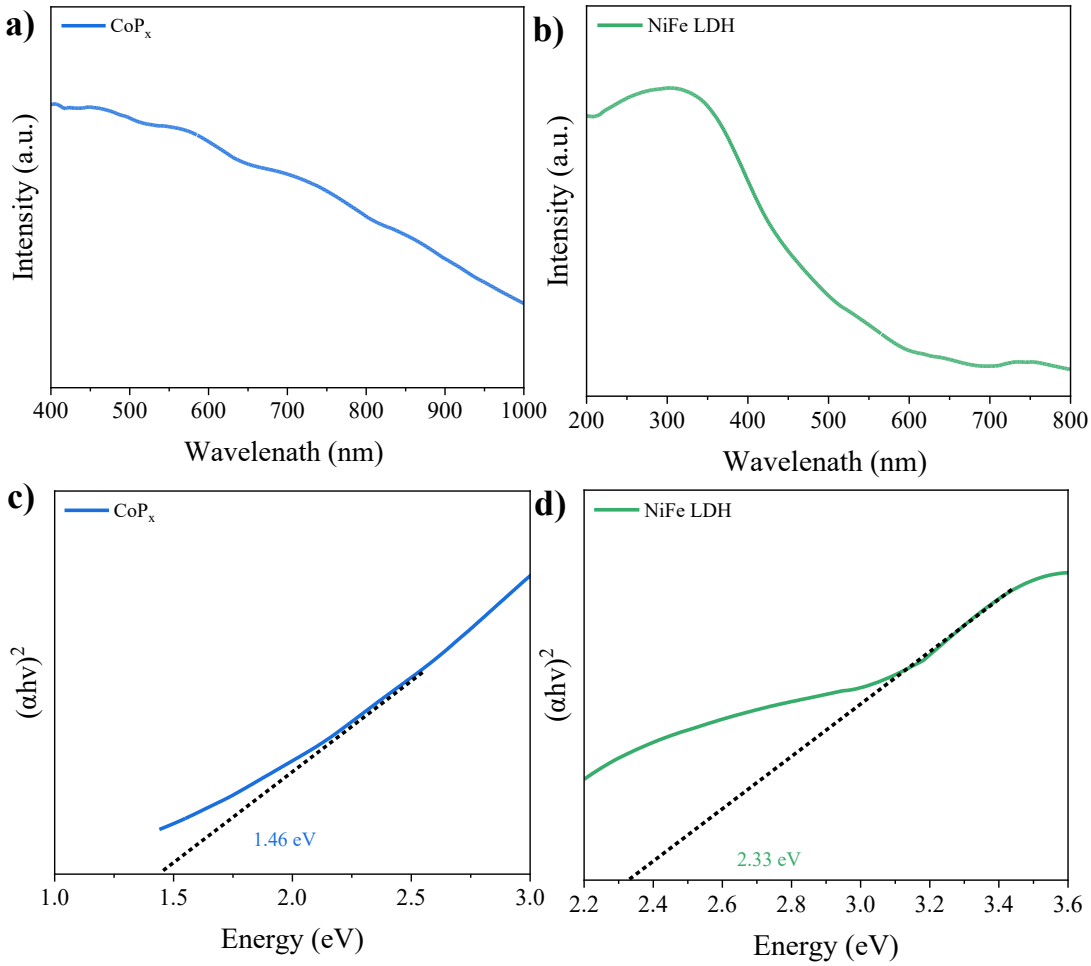

Fig. S13. NiFe LDH and CoP_x of (a-b) Ultraviolet-visible (UV-Vis) light absorption spectrum; (c-d) Tauc curves.

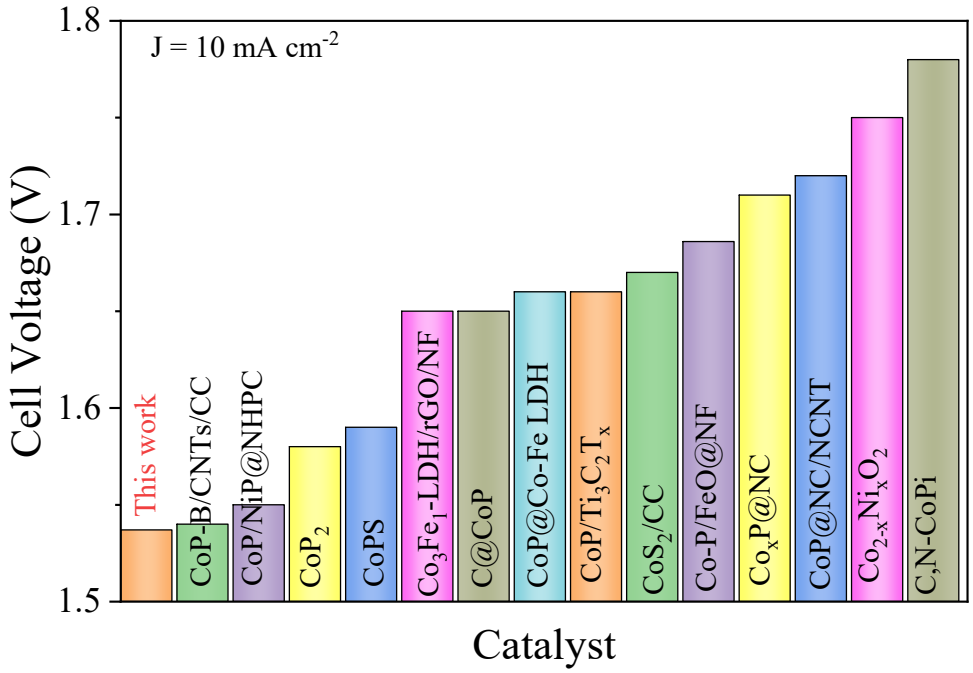

Fig. S14. The performance of the overall water-splitting reaction of other cobalt-based catalysts in a two-electrode system. [7, 8, 15, 17-27]

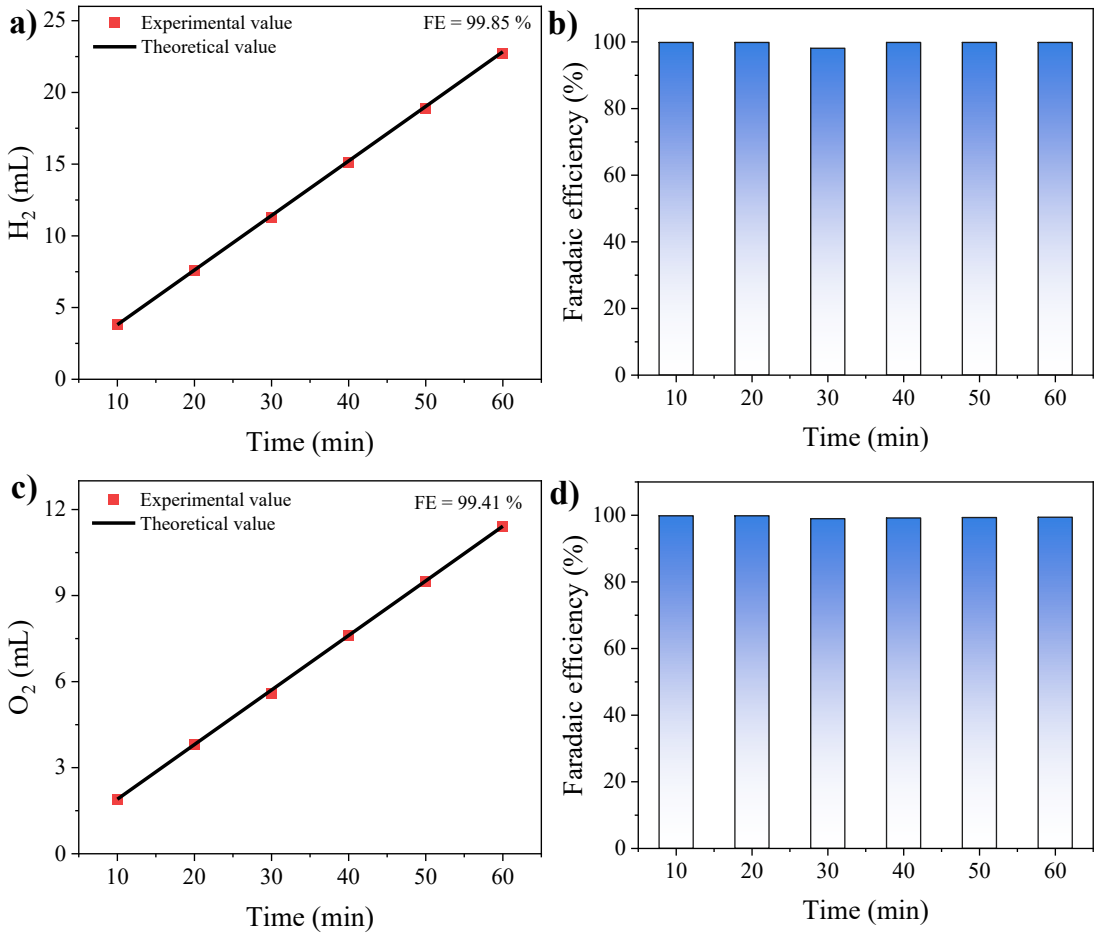

Fig. S15. Volume of collected gas a) H_2, c) O_2; Faraday efficiency of b) H_2, d) O_2.

Supplementary Note 1

After conducting the overall water splitting stability test at high current density, both the anodic (OER) and cathodic (HER) NiFe LDH/CoP_x electrodes were characterized using SEM and XPS to examine their morphological and chemical compositions, as well as oxidation states. Following the HER half-reaction test, the electrode morphology remained largely unchanged, as confirmed by the SEM image (**Fig. S16a**). However, after the OER half-reaction, a noticeable transformation was observed in the surface morphology, where the NiFe LDH nanosheets underwent reconstruction into smaller nanoparticles on the nanoporous CoP_x material (**Fig. S16b**). The XPS survey spectrum in **Fig. S17a** reveals that both the pre- and post-test electrodes are composed of five key elements: Ni, Fe, O, Co, and P. As shown in **Fig. S17b**, Ni predominantly exists in its divalent state (Ni^{2+}), indicating a reduction of Ni^{3+} to Ni^{2+} after the HER stability test, with only a slight decrease in peak intensity. In contrast, during the OER stability test, a small portion of the Ni^{2+} species was oxidized to Ni^{3+}, due to the formation of NiOOH, as evidenced by the increase in the corresponding Ni^{3+} peak. Similarly, the Fe 2p spectra (**Fig. S17c**) revealed a slight increase in the high-valence Fe species, indicating the oxidation of Fe^{2+} to Fe^{3+} during the OER stability test, while Fe remained stable during the HER half-reaction test.[28] In the O 1s spectrum (**Fig. S17d**), the dominant peak corresponding to M-OH suggests the formation of metal hydroxide layers on the surface of the hierarchical nanostructure after the OER stability test. On the other hand, the O 1s spectra after the HER stability test showed an increase in the M-O signal, indicating a shift towards metal oxide species. After the OER test, Co-related species exhibited higher valence states, attributed to the formation of Co-OOH and Co-PO_x (**Fig. S17e**).[16, 29] A slight negative shift in the Co^{2+} binding energy during the HER stability test can be attributed to the formation of Co-PO_x and Co-OH. Additionally, the P-Co peak disappeared after both the HER and OER stability tests, suggesting the dissolution or transformation of P-Co species.[30] Overall, these analyses indicate that the surface composition of the NiFe LDH/CoP_x heterostructure undergoes significant reconstruction during the stability tests. This results in the formation of

metal hydroxide/oxide phosphate active sites, which likely contribute to the enhanced catalytic activity and stability observed in the OER and HER reactions.[31]

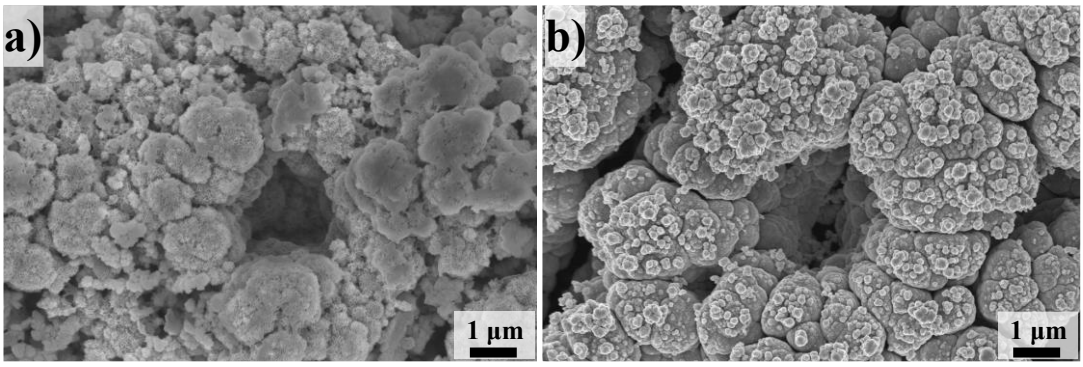

Fig. S16. SEM images of NiFe LDH/CoP_x as a) cathode and b) anode after stability test, respectively.

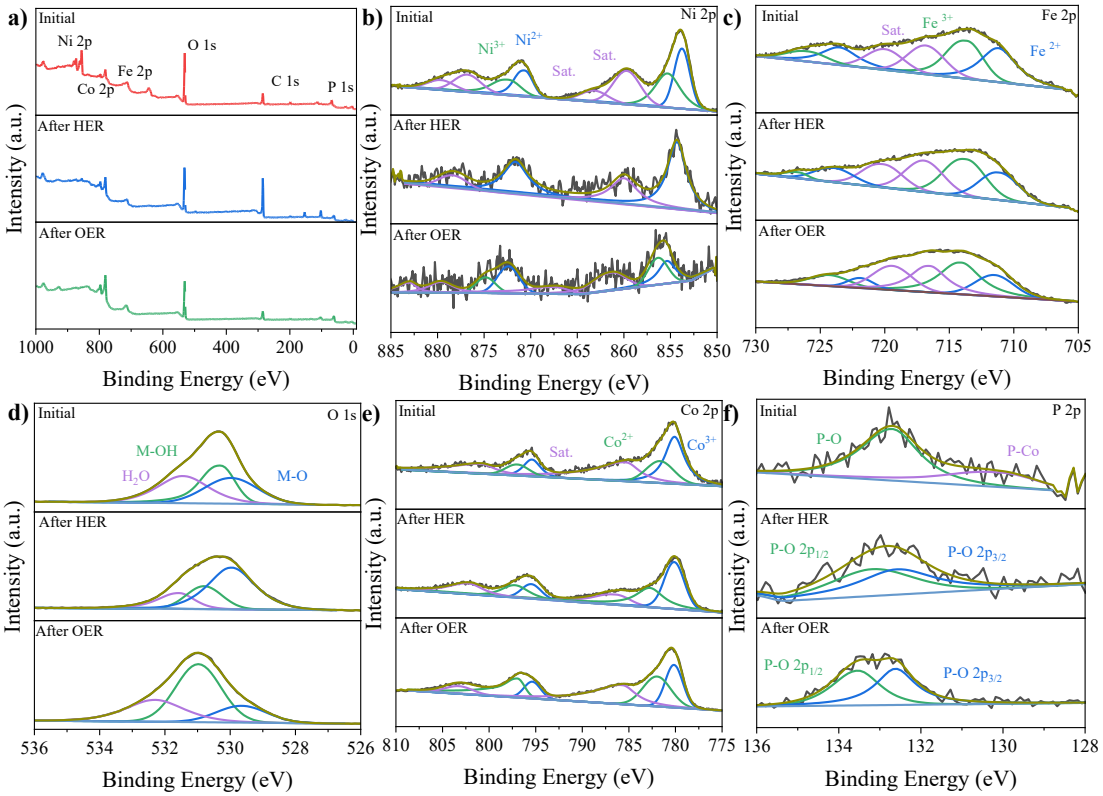

Fig. S17. XPS spectra of NiFe LDH/CoPx electrode before reaction, after HER stability test, and after OER stability test. a) XPS survey, b) Ni 2p, c) Fe 2p, d) O 1s, e) Co 2p, f) P 2p, respectively.

References

1. S. Tan, W. Ouyang, Y. Ji and Q. Hong, *Journal of Alloys and Compounds*, 2021, **889**, 161528.
2. J. Tong, Y. Li, L. Bo, W. Li, T. Li, Q. Zhang, D. Kong, H. Wang and C. Li, *ACS Sustainable Chemistry & Engineering*, 2019, **7**, 17432-17442.
3. M. Zhou, Q. Sun, Y. Shen, Y. Ma, Z. Wang and C. Zhao, *Electrochimica Acta*, 2019, **306**, 651-659.
4. D. Wei, L. Chen, L. Tian, S. Ramakrishna and D. Ji, *Industrial & Engineering Chemistry Research*, 2023, **62**, 4987-4994.
5. W.-Y. Zhu, X.-Z. Song, Y.-L. Meng, X. Chen, Z.-H. Wang, Y.-H. Zhao, T. Zhang, X.-F. Wang and Z. Tan, *Energy & Fuels*, 2021, **35**, 16760-16767.
6. H. Yang, B. Wang, S. Kou, G. Lu and Z. Liu, *Chemical Engineering Journal*, 2021, **425**, 131589.
7. B. Liu, P. Zhao, Z. Wu, C. Liu, H. Jing, J. Song, K. Lu, L. Wu and Q. Hao, *Journal of Colloid and Interface Science* 2024, **661**, 709-719.
8. G. H. Choi, J. Moon, E. Song, S. Cho, K. W. Park and J. T. Park, *International Journal of Energy Research*, 2022, **46**, 24633–24644.
9. M. Li, X. Wang, K. Liu, H. Sun, D. Sun, K. Huang, Y. Tang, W. Xing, H. Li and G. Fu, *Advanced Materials*, 2023, **35**, 2302462.
10. X. Lv, Z. Hu, J. Ren, Y. Liu, Z. Wang and Z.-Y. Yuan, *Inorganic Chemistry Frontiers*, 2019, **6**, 74-81.
11. Y. Gao, Z. Tong and X. Fan, *Electrochimica Acta*, 2021, **390**, 138797.
12. D. Rathore, S. Ghosh, J. Chowdhury and S. Pande, *ACS Applied Nano Materials*, 2022, **5**, 11823-11838.
13. S. Yuan, M. Xia, Z. Liu, K. Wang, L. Xiang, G. Huang, J. Zhang and N. Li, *Chemical Engineering Journal*, 2022, **430**, 132697.
14. J. Chang, F. Song, F. Xu, D. Wu, Y. Hou, K. Jiang, Y. Guo and Z. Gao, *Journal of Colloid and Interface Science*, 2024, **653**, 1063-1074.
15. C. Guan, X. Liu, A. M. Elshahawy, H. Zhang, H. Wu, S. J. Pennycook and W.

John, *Nanoscale Horizons*, 2017, **2**, 342-348.

16. H. Liu, Y. Zhang, R. Ge, J. M. Cairney, R. Zheng, A. Khan, S. Li, B. Liu, L. Dai and W. Li, *Applied Energy*, 2023, **349**, 121582.
17. M. Zhang, J. Tu, M. Li and L. Zhi, *Journal of Electroanalytical Chemistry*, 2024, **961**, 118224.
18. M. Wang, C.-L. Dong, Y.-C. Huang and S. Shen, *Journal of Catalysis*, 2019, **371**.
19. W. Li, G. Cheng, M. Sun, Z. Wu, G. Liu, D. Su, a. Bang Lan, S. Mai, L. Chen and Y. Lin, *Nanoscale*, 2019, **11**, 17084.
20. J. Liu, G. Chen, J. Xiao and Y. Zhang, *International Journal of Hydrogen Energy*, 2024, **62**, 803-811.
21. Z.-Q. Huang, W.-X. Lu, B. Wang, W.-J. Chen, J.-L. Xie, D.-S. Pan, L.-L. Zhoua and J.-L. Song, *Catalysis Science & Technology*, 2019, **9**, 4718-4724.
22. J.-S. Li, L.-X. Kong, Z. Wu, S. Zhang, X.-Y. Yang, J.-Q. Sha and G.-D. Liu, *Carbon*, 2019, **145** 694-700.
23. Z. Wu, B. Liu, H. Jing, H. Gao, B. He, X. Xia, W. Lei and Q. Hao, *Journal of Colloid and Interface Science*, 2023, **629**, 22-32.
24. R. Guo, J. Shi, K. Ma, W. Zhu, H. Yang and M. Sheng, *Journal of Colloid and Interface Science*, 2023, **651**, 172-181.
25. J. Guo, Z. Wei, K. Wang and H. Zhang, *International Journal of Hydrogen Energy*, 2021, **46**, 27529-27542.
26. H. Li, L. Chen, P. Jin, H. Lv, H. Fu, C. Fan, S. Peng, G. Wang, J. Hou, F. Yua and Y. Shi, *Dalton Transactions*, 2020, **49**, 6587.
27. G. Hu, J. Xiang, J. Li, P. Liu, R. N. Ali and B. Xiang, *Journal of Catalysis*, 2019, **371**, 126-134.
28. Y.-F. Chen, J.-H. Li, T.-T. Liu, S.-H. You, P. Liu, F.-J. Li, M.-Q. Gao, S.-G. Chen and F.-F. Zhang, *Rare Metals*, 2023, **42**, 2272-2283.
29. X. Qin, B. Yan, D. Kim, Z. Teng, T. Chen, J. Choi, L. Xu and Y. Piao, *Applied Catalysis B: Environmental*, 2022, **304**, 120923.

30. Y. Liu, Z. Zhang, L. Zhang, Y. Xia, H. Wang, H. Liu, S. Ge and J. Yu, *Journal of Materials Chemistry A*, 2022, **10**, 22125-22134.

31. H. Zhang, X. Li, A. Hähnel, V. Naumann, C. Lin, S. Azimi, S. L. Schweizer, A. W. Maijenburg and R. B. Wehrspohn, *Advanced Functional Materials*, 2018, **28**, 1706847.